Realization of the Meminductor

Jiahao Han, Cheng Song,* Shuang Gao, Yuyan Wang, Chao Chen, and Feng Pan

Key Laboratory of Advanced Materials (MOE), School of Materials Science and Engineering, Tsinghua University, Beijing 100084, China

ABSTRACT The meminductor was proposed to be a fundamental circuit memdevice parallel with the memristor, linking magnetic flux and current. However, a clear material model or experimental realization of a meminductor has been challenging. Here we demonstrate pinched hysteretic magnetic flux–current signals at room temperature based on the spin Hall magnetoresistance effect in several-nanometer-thick thin films, exhibiting the nonvolatile memorizing property and magnetic energy storage ability of the meminductor. Similar to the parameters of the capacitor, resistor, and inductor, meminductance, L_M, is introduced to characterize the capability of the prepared meminductor. Our findings present an indispensable element of memdevices and open an avenue for nanoscale meminductor design and manufacture, which might contribute to low-power electronic circuits, information storage, and artificial intelligence.

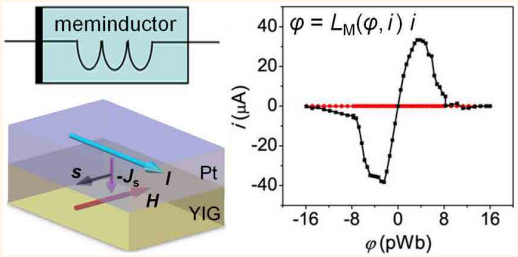

KEYWORDS: meminductor · the spin Hall magnetoresistance effect · magnetic flux · electric current · pinched hysteretic curve

There are four fundamental circuit variables, namely, electric current i, voltage v, charge q, and magnetic flux φ, and three fundamental passive elements are currently used to build electronic circuits: the capacitor connects voltage and charge, the resistor connects voltage and current, and the inductor connects magnetic flux and current. In 1971, Chua[1] proposed the memristor as the fourth element to provide a functional relation between magnetic flux and charge, establishing its fundamental position in electronic circuits. The memristor is a two-terminal device whose voltage–current curve is a pinched hysteresis with high and low resistance states.[2] Also, the memristor remembers the most recent resistance value when the input current is turned off and until the next time the input current is turned on.[3−5] Soon afterward, the concept of the memristor was expanded to illustrate memristive systems as a broad generalization.[5,6] In 2008, Strukov *et al.*[7] observed hysteretic voltage–current loops when investigating $Pt/TiO_2/Pt$ resistive switching devices. Although magnetic signals are not applied or measured, the resistive switching device is considered a typical memristor due to its pinched voltage–current curves for remembering the resistance.[8−11] Owing to its nonvolatile memorizing ability, the memristor has a great potential in commercial application as the coming generation of memories and digital circuits without shrinking transistors, thus possibly changing the dominant principle of electronic industry, i.e., Moore's law.[12,13]

On the basis of symmetry, the notion of memristive systems was extended to capacitive and inductive elements, namely, capacitors and inductors, whose properties depend on the state and history of the systems, called meminductors and memcapacitors (Figure 1a). All these elements typically show pinched hysteretic loops in the two constitutive variables that define them. The meminductor, defined by a state-dependent relation between magnetic flux and current, $\varphi = L_M(\varphi,i)i$, where $L_M(\varphi,i)$ represents meminductance as a function of magnetic flux φ and current i through the device, should exhibit a pinched hysteresis loop in the magnetic flux–current plane when subjected to a bipolar periodic signal.[14] Actually, the meminductor is not new, but was a member of the periodic table of elements published by Chua in the 1980s.[15,16] It can remember its most recent inductance value when the input current is turned off and until the next time the input current is turned on. In this case, the meminductor is expected to play an important role in low-power electronic circuits because of its energy storage capability.[17]

To fulfill the requirements above, we design a meminductor on the basis of the spin

* Address correspondence to songcheng@mail.tsinghua.edu.cn.

Received for review May 15, 2014 and accepted September 26, 2014.

Published online September 26, 2014
10.1021/nn502655u

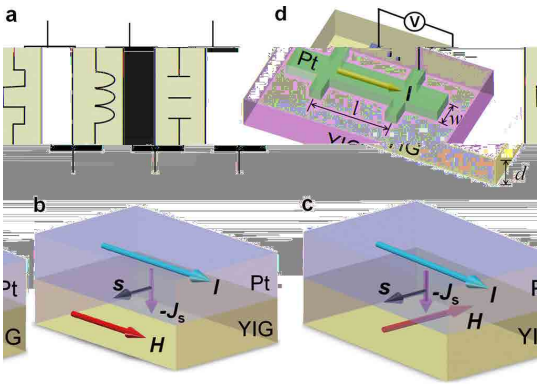

Figure 1. Schematics of the memory system and the SMR effect. (a) Schematic of the memristor (left), meminductor (middle), and memcapacitor (right). (b) High resistance state in the SMR effect of the Pt/YIG bilayer. (c) Low resistance state in the SMR effect of the Pt/YIG bilayer. (d) Schematic of the sample layout.

Hall magnetoresistance (SMR) effect in a Pt film attached to an insulating $Y_3Fe_5O_{12}$ (YIG) ferrimagnet.[18] The mechanism of the SMR effect can be understood as follows: the flow of electrons *I* in the Pt layer deflects upward and downward, ascribed to spin−orbit coupling. When the magnetization of the YIG is perpendicular (parallel) to the spin polarization *s*, the spin current J_s is absorbed maximally (minimally) by the magnetization as a spin Hall torque absorption, as illustrated in Figure 1b and c.[19,20] The low absorption means that the electrons arriving at the Pt/YIG interface are largely reflected back into the Pt layer and form an additional current driven by the spin−obit coupling acting as the electromotive force, as a part of the input current, thus resulting in a low resistance state (Figure 1c).

RESULTS AND DISCUSSION

We have investigated the SMR effect for 3, 5, and 7 nm thick Pt films grown on YIG films. As expected, the room-temperature hysteresis loop of the YIG in Figure 2a exhibits its ferrimagnetic feature with a low saturation field of ~5 mT. A schematic of the sample layout is shown in Figure 1d. Corresponding magnetoresistance curves at room temperature are presented in Figure 2b, c, and d. Although the conductive electrons in the Pt film cannot enter the magnetic insulator, the resistance of the Pt film reflects the magnetization direction of the YIG. The magenetoresistance curve for the field ramping down from positive to negative cannot be separated clearly from its counterpart with the field up-sweeping taking the small coercivity (~0.3 mT) of the YIG into account. The most eminent result here is that the high and low resistances are observed at zero field and high field, respectively, with an SMR ratio of $\sim 10^{-2}$%. The transition field coincides with the saturation field of the hysteresis loop displayed in Figure 2a. These behaviors are quite characteristic for the SMR effect.[18] The magnetization of the

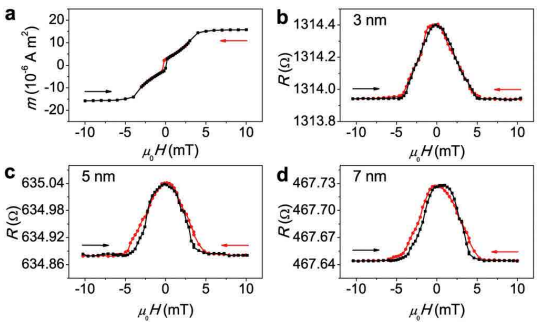

Figure 2. Spin Hall magnetoresistance of Pt films grown on YIG. (a) Hysteresis loop [moment (*m*)−field ($\mu_0 H$)] of a plain YIG film. (b, c, and d) Magnetoresistance curves of the Pt films with thicknesses of 3, 5, and 7 nm, respectively. All the curves are measured at 300 K.

YIG manipulates the proportion of the driven part and normal part in the channel current. Subsequently, the decrease of the resistance is dominated by the increase of the driven current reflected from the Pt/YIG interface. Note that the magnitude of the SMR signal (the difference between the high and low resistance states) drops abruptly as the Pt film thickness is increased, *i.e.*, 0.45, 0.16, and 0.08 Ω for 3, 5, and 7 nm thick Pt samples, respectively. The SMR effect, reflecting the dependence of the channel resistance on the magnetization, is expected to establish the relation between magnetic flux and current, thus providing an approach to realizing a meminductor.

Thus we present the designing process of the meminductor. A sinusoidal current is input into the Hall bar along the longitudinal direction. The current itself generates a transverse static magnetic field in the YIG, the direction of which is the same as the applied magnetic field in the SMR experiments. If the peak value of the input current is large enough, the generated static magnetic field will saturate the magnetization of the YIG layer. In this way the current could manipulate the resistance of the Pt channel directly without external magnetic fields. Meanwhile, magnetic energy is generated by the current and stored due to the magnetization of YIG. We then take the 3 nm thick Pt sample as an example. A periodic sinusoidal current $I = 800 \sin(2\pi t/T)$ (mA) is input for the generation of the magnetic field, where *t* is the time during which the current is input and *T* is the time used for recording a hysteresis loop (917 s in our case), as displayed in the upper panel of Figure 3a.

In our case, the Pt film can be regarded as an infinite plane taking the channel width *w* of 50 μm and the film thickness of several nanometers into account. Thus, the relation between magnetic field $\mu_0 H$ and current *I* is $\mu_0 H = \mu_0 I/2w$. The peak value of the current is calculated to be ~800 mA for generation of the maximal magnetic field of 10 mT. Subsequently, the SMR effect performed in a magnetic field can be changed to the resistance as a function of applied current. It should be

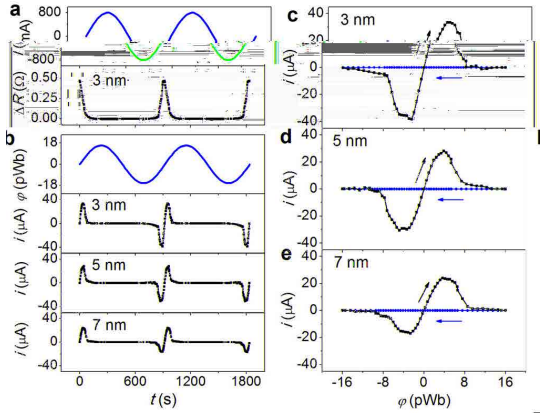

Figure 3. Nonvolatile hysteretic magnetic flux−current curves. (a) Time-dependent resistance difference ΔR for the 3 nm thick Pt sample associated with the sinusoidal input current $I = 800 \sin(2\pi t/T)$ (mA), where T equals 917 s. The bias magnetic field is set at 20 and 0 mT as the input current decreases and increases, respectively. (b) Magnetic flux φ generated by the input current I and the varied current i of the 3, 5, and 7 nm thick Pt samples as a function of time t. (c, d, and e) Magnetic flux−current curves obtained in 3, 5, and 7 nm thick Pt films, respectively.

noted that such a large current is only proposed to be used in our proof-of-concept devices with a channel width of 50 μm and is not fundamentally necessary for typical nanoelectronics (*e.g.*, 22 nm width). When the in-plane dimensions of the device are on the nanoscale, the input current I and the resistance R of the device decrease abruptly. Subsequently, the thermal effects estimated by I^2R are expected to be significantly reduced. Meanwhile, the size effect and the dipolar coupling between neighboring cells should not be the obstacle for high-density integration of the present device due to its working field being lower than 10 mT, comparable to that of magnetoresistive random access memory.[21]

Given that the meminductor does not belong to the four fundamental elements,[17] the analytical process of realizing a meminductor is expected to be more complicated than that of the memristor.[7] To separate the SMR signal, a transverse bias magnetic field is applied as a function of the sinusoidal current: it stays at a field larger than the field for the SMR measurements when the current decreases (20 mT is selected here), while it switches to zero as the current increases. Alternatively, the function of the external magnetic field can be implemented by a series circuit composed of a capacitor and a diode (1C1D), which is in parallel with the meminductor (Pt/YIG). The diode determines ON/OFF states of the 1C1D subcircuit, where the current shows a 90° phase difference from that through the meminductor, guaranteeing ON and OFF magnetic fields are applied to the meminductor, similar to the scenario in Figure 3a. Nevertheless, we still use the external field below in the analytical process for simplicity. In this scenario, the SMR effect in Figure 2b can be repeated by time (t)-dependent longitudinal resistance difference ΔR by combining the sinusoidal input current and transverse bias magnetic field, as plotted in the bottom panel of Figure 3a, in which the resistance difference ($\Delta R = R - R_{low}$, where R_{low} represents the minimum resistance value) between the high and low resistance is used to highlight the variation and to remove the giant resistance background (~1313.9 Ω).

The resistance difference ($\Delta R-t$) associated with the instantaneous current input ($I-t$) as a function of time is then used to illustrate the magnetic flux−current ($\varphi-i$) curve of the meminductor. In our case, φ represents the flux of the magnetic field $\mu_0 H$ through the side face of the YIG layer, which is directly generated by the input current I; that is, $\varphi = \mu_0 HS = \mu_0 Ild/2w$, where l and w represent the length and width of the Pt Hall bar and d represents the thickness of the YIG layer (Figure 1d). Meanwhile, the current i is defined as the varied current, besides the current background, which is never manipulated by the spin−orbit coupling under the magnetic field, reflecting the strength of the current variation relevant to the Pt/YIG interface. Hence, i is expressed by $i = I(R - R_{low})/R_0$, where I is the input current and R_{low} and R_0 parameters are the minimum and maximum value of the resistance, *e.g.*, 1313.9 and 1314.4 Ω for the 3 nm thick Pt sample, respectively. Accordingly, the magnetic flux ($\varphi-t$) and the varied current ($i-t$) of the 3 nm thick Pt sample as a function of time are obtained, as shown in the upper panels of Figure 3b, which serve as the basis for the magnetic flux−current curve. Obviously, the flux and current curves cross each other at zero flux and zero current.

As displayed in Figure 3c, it is noteworthy that the magnetic flux−current ($\varphi-i$) curve is transversal pinched at the origin, which constitutes the main finding of our work. This feature ensures the present SMR meminductor is a nonvolatile memory device that retains its inductance even when the power is interrupted.[22,23] If the current is turned off when it is increasing, the meminductor presents a low inductance state. Actually, a high-density, high-speed, and low-power nonvolatile memory has been expected in the semiconductor industry for a long time, which may lead to computer systems that do not require a lengthy start-up process when turned on.[24] In the bottom panels of Figure 3b, $i-t$ curves of the 5 and 7 nm thick Pt samples are displayed. Concomitant magnetic flux−current signals obtained in these Pt samples show the same qualitative behavior as the 3 nm thick Pt sample, but with a reduced overall magnitude (Figure 3d and e), indicating the critical role of the nanoscale region close to the YIG/Pt interface. The peak values of the current signals are inversely proportional to the Pt film thickness, suggesting that the capability of the meminductors is quite sensitive to their design parameters, which will be discussed below.

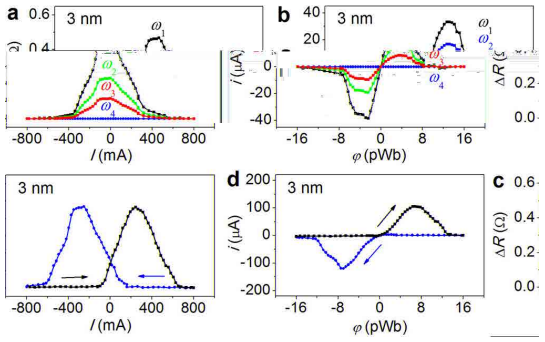

Figure 4. Frequency-dependent nonvolatile hysteretic magnetic flux−current curves and volatile hysteretic magnetic flux−current curves. (a) Sketched $I-\Delta R$ curves of the 3 nm thick Pt sample for different frequencies ω ($\omega_1 < \omega_2 < \omega_3 < \omega_4$) of the input current, where ω_1 is identical to the field scanning frequency in our measurements, ω_2 and ω_3 are on the scale of the spin-dependent scattering time (∼ns), and ω_4 approaches infinity as a limit. (b) Corresponding magnetic flux−current curves for different frequencies. (c) Relationship between the input current I and the longitudinal resistance difference ΔR of the 3 nm thick Pt film. The bias magnetic field is set at 3 and −3 mT as the input current decreases and increases, respectively. (d) Magnetic flux−current curve obtained in the 3 nm thick Pt film in accordance with (c).

The situation changes as the current frequency increases dramatically. If the input current period is quite short, comparable with the spin-dependent scattering time (∼ns),[25,26] the electrons driven by spin−orbit coupling in the Pt layer could not complete a whole deflection process during such a short current period, resulting in the remarkable change of the SMR signals. In this scale, with the increase of the frequency ω, the resistance difference ΔR would be greatly reduced (Figure 4a), and the corresponding hysteretic behavior of the magnetic flux−current curves becomes less distinct (Figure 4b). Particularly, when the frequency of the input current approaches infinity as a limit, there is not enough time for any spin-dependent scattering, and the present hysteretic magnetic flux−current curve shrinks into a single-valued one. The meminductor degenerates into an ordinary inductor.[22]

In addition to the nonvolatile magnetic flux−current loops, we have explored their volatile counterparts by applying different bias magnetic fields. For this modeling, the bias magnetic field is set to be 3 and −3 mT as the input current decreases and increases, respectively. This bias field leads to the horizontal separation of the SMR curves in Figure 2b. A resultant $I-\Delta R$ curve for the 3 nm thick Pt sample is displayed in Figure 4c. Accordingly, a concomitant magnetic flux−current curve in Figure 4d exhibits a nontransversal pinched feature. Remarkably, its inductance state depends on the sign of magnetic flux φ and $d\varphi/dt$ at the time before the applied current is turned off. As they possess the same sign, the device is in a low inductance state, and *vice versa*. However, in this case it exhibits a volatile

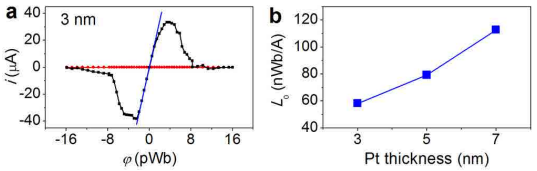

Figure 5. Calculation of memristance. (a) Magnetic flux−current curve of the 3 nm thick Pt sample. The value of L_0 is defined at the reciprocal of the tangent slope at the origin. (b) Dependence of L_0 on the thickness of the Pt films.

behavior, contrary to the scenario of the transversal pinched one. It is also found that this volatile case can be achieved without a bias magnetic field. If the YIG film has a sizable coercivity, such as 3 mT already achieved in previous YIG films,[19] the peak resistance would deviate naturally from the $I = 0$ point. Subsequently, a volatile magnetic flux−current curve similar to the one in Figure 4d could be obtained.

We now turn to the calibration of meminductance L_M to characterize the capability of the prepared meminductor with the mathematical relation $\varphi = L_M i$, which is significant not only for basic understanding of the element but also for device application. Obviously, the slope of the line connecting the origin and the point on the magnetic flux−current curve corresponds to the reciprocal of meminductance L_M at each point. Accordingly, L_M is a magnetic flux- and current-dependent variable, reflecting the essential feature of the meminductor as a nonlinear dynamical circuit element and the significant effect of magnetic flux and current, which is in sharp contrast to the constant parameters C, R, and L for the capacitor, resistor, and inductor, but consistent with the charge- and current-dependent memristance M for the memristor (unclear yet).[3] We note that it is inconvenient to use a complicated variable to characterize the capability of a meminductor, so the reciprocal of the slope of the tangent line at the origin, referred to as L_0, is employed to calibrate the memristance L_M (Figure 5a). L_0 equals 58, 79, and 113 nWb/A for the 3, 5, and 7 nm thick Pt samples, respectively. To some extent L_0 scales proportionally to the Pt film thickness with a certain input current (Figure 5b), although the shape of the magnetic flux−current loops and L_0 vary with the amplitude and the frequency of the input current.[27] Therefore, the thickness of the Pt film plays a dominant role on the parameter of the meminductor, including the value of L_0 and the functional relation between L_M and magnetic flux as well as current. Once a certain value of L_0 is provided for a fabricated meminductor, the magnetic flux−current loops could be fixed when applying this meminductor in electronic circuits.

CONCLUSIONS

Our results demonstrate a meminductor based on the spin Hall magnetoresistance effect in the Pt/YIG bilayers, exactly described by the mathematical relation

between magnetic flux and current, $\varphi = L_M i$. When the meminductor is working, the input current magnetizes the YIG film and manipulates the magnitude of the Pt resistance, forming pinched hysteretic magnetic flux−current loops. Thus, the meminductor works as a typical nonvolatile memory that retains its data even after the power is turned off, and magnetic energy is stored due to the magnetization of YIG, which might advance the development of self-powered electronic circuits. The capability of the meminductor is characterized by meminductance L_M, guaranteeing the labeling of a manufactured meminductor with a certain value of L_0. Besides the fundamental significance, the meminductor, in conjunction with the already known memristor and the unrealized memcapacitor, would provide a rich platform for analog circuits, information storage, and artificial intelligence.

METHODS

SMR Device Preparation. The SMR effect was measured with Pt Hall bars grown on YIG substrates. Pt films with a thickness of 3, 5, and 7 nm were deposited on highly insulating single-crystalline (111) YIG films by magnetron sputtering at room temperature. The thickness of the YIG films (d) is 4 μm. The Pt Hall bar with a width w of 50 μm and a length l of 400 μm was made by standard lithographic techniques for transport measurements.

SMR Measurements. The longitudinal resistance R of the Pt Hall bars was measured by a four-point contact geometry with a constant channel current I of 100 μA at 300 K when an in-plane magnetic field H perpendicular to I was swept from 10 mT to −10 mT and then back to 10 mT, using the Physical Property Measurement System by Quantum Design in resistivity mode.

Conflict of Interest: The authors declare no competing financial interest.

Acknowledgment. The authors thank Prof. H. W. Zhang and Dr. Q. H. Yang for providing some of the YIG wafers and H. Y. Yu at the Center for Testing and Analyzing of Materials for technical support. This work was supported by the National Natural Science Foundation of China (Grant Nos. 51322101, 51202125, and 51231004) and National Hi-tech (R&D) Project of China (Grant Nos. 2014AA032901 and 2014AA032904).

REFERENCES AND NOTES

1. Chua, L. O. Memristor−the Missing Circuit Element. *IEEE Trans. Circuit Theory* **1971**, *18*, 507–519.
2. Prodromakis, T.; Toumazou, C.; Chua, L. O. Two Centuries of Memristors. *Nat. Mater.* **2012**, *11*, 478–481.
3. Mohanty, S. P. Memristor: from Basics to Deployment. *IEEE Potentials* **2013**, *32*, 34–39.
4. Chua, L. O.; Kang, S. M. Memristive Devices and Systems. *Proc. IEEE* **1976**, *64*, 209–223.
5. Chua, L. O. Resistive Switching Memories are Memristors. *Appl. Phys. A* **2011**, *102*, 765–783.
6. Chua, L. O. If It's Pinched It's a Memristor. In *Memristor and Memristive Systems*; Tetzlaff, R., Ed.; Springer: New York, 2014; pp 33−100.
7. Strukov, D. B.; Snider, G. S.; Stewart, D. R.; Williams, R. S. The Missing Memristor Found. *Nature* **2008**, *453*, 80–83.
8. Mathur, N. D. The Fourth Circuit Element. *Nature* **2008**, *455*, E13.
9. Pan, F.; Gao, S.; Chen, C.; Song, C.; Zeng, F. Recent Progress in Resistive Random Access Memories: Materials, Switching Mechanisms, and Performance. *Mater. Sci. Eng. R* **2014**, *83*, 1–59.
10. Liu, Q.; Long, S. B.; Lv, H. B.; Wang, W.; Niu, J. B.; Huo, Z. L.; Chen, J. N.; Liu, M. Controllable Growth of Nanoscale Conductive Filaments in Solid-Electrolyte-Based ReRAM by Using a Metal Nanocrystal Covered Bottom Electrode. *ACS Nano* **2013**, *4*, 6162–6168.
11. Chai, Y.; Wu, Y.; Takei, K.; Chen, H.-Y.; Yu, S.; Chan, P. C. H.; Javey, A.; Wong, H.-S. P. Nanoscale Bipolar and Complementary Resistive Switching Memory Based on Amorphous Carbon. *IEEE Trans. Electron Devices* **2011**, *58*, 3933–3939.
12. Kim, S.; Choi, S.; Lu, W. Comprehensive Physical Model of Dynamic Resistive Switching in an Oxide Memristor. *ACS Nano* **2014**, *8*, 2369–2376.
13. Williams, R. S. How We Found the Missing Memristor. *IEEE Spectr.* **2008**, *45*, 29–35.
14. Ventra, M. D.; Pershin, Y. V.; Chua, L. O. Circuit Elements with Memory: Memristors, Memcapacitors, and Meminductors. *Proc. IEEE* **2009**, *97*, 1717–1724.
15. Chua, L. O. Nonlinear Circuit Foundations for Nanodevices, Part I: The Four- Element Torus. *Proc. IEEE* **2003**, *91*, 1830–1859.
16. Chua, L. O. The Fourth Element. *Proc. IEEE* **2012**, *100*, 1920–1927.
17. Ventra, M. D.; Pershin, Y. V.; Chua, L. O. Putting Memory into Circuit Elements: Memristors, Memcapacitors, and Meminductors. *Proc. IEEE* **2009**, *97*, 1371–1372.
18. Nakayama, H.; Althammer, M.; Chen, Y.-T.; Uchida, K.; Kajiwara, Y.; Kikuchi, D.; Ohtani, T.; Geprags, S.; Opel, M.; Takahashi, S.; *et al*. Spin Hall Magnetoresistance Induced by a Nonequilibrium Proximity Effect. *Phys. Rev. Lett.* **2013**, *110*, 206601.
19. Althammer, M.; Meyer, S.; Nakayama, H.; Schreier, M.; Altmannshofer, S.; Weiler, M.; Huebl, H.; Geprags, S.; Opel, M.; Gross, R.; *et al*. Quantitative Study of the Spin Hall Magnetoresistance in Ferromagnetic Insulator/Normal Metal Hybrids. *Phys. Rev. B* **2013**, *87*, 224401.
20. Vlietstra, N.; Shan, J.; Castle, V.; van Wees, B. J.; Youssef, J. B. Spin-Hall Magnetoresistance in Platinum on Yttrium Iron Garnet: Dependence on Platinum Thickness and In-Plane/Out-of-Plane Magnetization. *Phys. Rev. B* **2013**, *87*, 184421.
21. Ikeda, S.; Miura1, K.; Yamamoto, H.; Mizunuma, K.; Gan, H. D.; Endo, M.; Kanai, S.; Hayakawa, J.; Matsukura, F.; Ohno, H. A Perpendicular-Anisotropy CoFeB−MgO Magnetic Tunnel Junction. *Nat. Mater.* **2010**, *9*, 721–724.
22. Adhikari, S. P.; Sah, M. P.; Kim, H.; Chua, L. O. Three Fingerpoints of Memristor. *IEEE Trans. Circuits Syst.* **2013**, *60*, 3008–3021.
23. Kim, H.; Sah, M. P.; Adhikari, S. P. Pinched Hysteresis Loops is the Fingerpoint of Memristor Devices. http://arXiv.org/abs/1202.2437.
24. Meijer, G. I. Materials Science. Who Wins the Nonvolatile Memory Race?. *Science* **2008**, *319*, 1625–1626.
25. Song, C.; Sperl, M.; Utz, M.; Ciorga, M.; Woltersdorf, G.; Schuh, D.; Bougeard, D.; Back, C. H.; Weiss, D. Proximity Induced Enhancement of the Curie Temperature in Hybrid Spin Injection Devices. *Phys. Rev. Lett.* **2011**, *107*, 056601.
26. Nagaosa, N.; Sinova, J.; Onoda, S.; MacDonald, A. H.; Ong, N. P. Anomalous Hall Effect. *Rev. Mod. Phys.* **2010**, *87*, 1539–1591.
27. Adhikari, S. P.; Kim, H. Why are Memristor and Memistor Different Devices?. *IEEE Trans. Circuits Syst.* **2013**, *59*, 2611–2618.